Robust Controller Design for Phase-Shifted Full-Bridge Series Resonant Converter under the Nonlinear Load

Sungho Son[1], Minsung Kim[2], Sungho Lee[3], and Jin S. Lee[1]
[1] Department of Creative IT Engineering, POSTECH.
[2] Future IT Research Laboratory, POSTECH.
[3] Department of Electrical Engineering, POSTECH.
77 Cheongam-Ro. Nam-Gu. 790-784
Pohang, Republic of Korea
Email: sungho22@postech.ac.kr

Keywords

Sliding mode control, Non-linear control, Resonant converter.

Abstract

In this paper, a third-order sliding mode control (3-SMC) scheme is proposed for the phase-shifted full-bridge series resonant converter (PSFB-SRC) which has a nonlinear characteristic and experiences the nonlinear load variation when it is used in DC/DC power supply application. 3-SMC is effective in compensating the nonlinear load variation in nonlinear system. The system modeling of resonant tank and output filter are derived, and the 3-SMC which is comprised of an equivalent controller and a switching controller is developed. Numerical simulations are performed to validate the proposed control approach.

Introduction

Full-bridge type converters are widely used to transfer large amounts of power in DC/DC power supply application. Among the various full bridge type converters [1, 2], the phase-shifted full-bridge series resonant converter (PSFB-SRC) has drawn a great attention because it has a high conversion efficiency [2], and the transformer used in the converter does not easily saturate due to a series connection between the resonant capacitor and the transformer winding. However, the control of the PSFB-SRC is difficult due to its nonlinear characteristic. Furthermore, when it is used in DC/DC power supply application, it may experience nonlinear load variation within a specific range. Precise control of output voltage is very important because the high ripple of output voltage induces large power reduction [3] and causes burden to power supply such as fuel-cell aging [4].

Considerable research has been conducted to address these problems, and various robust control strategies have been proposed to be used for a PSFB-SRC and with nonlinear loads [5, 6, 7] in the literatures. Zero-current switching (ZCS), zero-voltage switching (ZVS) [8, 9, 10], pulse-width modulation (PWM) with phase shift [11] and proportional-integral control [12] to balancing the output voltage are the primary control for the switching signal. An adaptive feedback regulation scheme is proposed for the stabilization of average models of dc-to-dc power converters exhibiting unknown but constant resistive loads. [13]. A Quantitative feedback theory approach is proposed to provide robust performance such as fast disturbance rejetion under wide load variation [14]. However, the performance of these controller depends on the accuracy of the plant model a complicated computation is required. The adaptive control such as auto-disturbance-rejection control (ADRC) where the load variation is observed and estimated by an extended state observer [15] and passivity-based control which ensures that the closed-loop system is exponentially convergent and only a single output feedback is required [16] are also proposed.

Among the aforementioned controllers, sliding mode control (SMC) has attracted significant attention due to its simple structure and robustness to uncertain dynamics and unknown disturbances. However, in practical systems, the standard SMC may suffer from high frequency oscillations due to the discontinuous switching control action. To decrease these high frequency oscillations, which is called a chattering phenomenon, simple rule which makes the trajectory stay within predetermined boundary layer was developed in [17]; continuous functions such as saturation functions, hyperbolic functions and hysteresis-saturation functions were used instead of discontinuous function in switching action in [18].

Another formulation for the sliding variable, based on the high-order sliding mode concept, was introduced in [19, 20, 21]. The control scheme with this sliding variable is called a high-order sliding mode controller. Since it incorporates the knowledge about the high-order derivative of the sliding surface, it can reduce the chattering phenomenon. In this paper, we propose the use of third-order sliding mode controller (3-SMC) for PSFB-SRC, in which the performance improvement in steady-state response under the load variation is shown. PSFB-SRC consists of resonant tank system and output filter system. We derived modeling of resonant tank system and output filter system. And then, we developed 3-SMC for PSFB-SRC, which consists of three components: a linear controller keeps the closed-loop system within a uniform bound; a nonlinear cancellation term cancels the nonlinear part of the resonant tank, and a switching controller compensates for a steady-state error and suppresses the remaining bias term. We performed numerical simulations to test the performance of the proposed 3-SMC.

In the subsequent discussion, we will use the following notation and definitions. R^n is the n-dimensional Euclidean space over R. A hat over a variable (i.e. $\hat{(\cdot)}$) denotes the estimated value of $(\cdot)$ and $\equiv$ denotes *is defined as*. The signum function $\mathrm{sgn}(\cdot)$ is defined as

$$\mathrm{sgn}(x) \equiv \begin{cases} -1 & \text{if} \quad x < 0 \\ 0 & \text{if} \quad x = 0 \\ 1 & \text{if} \quad x > 0 \end{cases}, \tag{1}$$

where x is scalar variable.

Modeling of the converter

System description

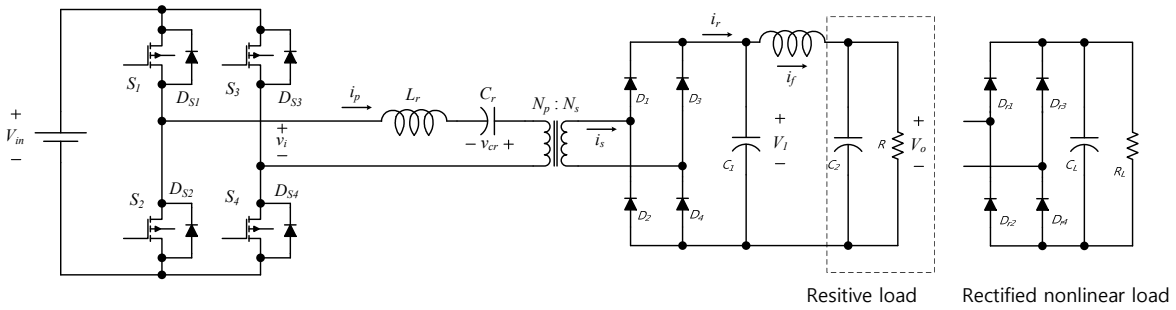

Figure 1: The circuit diagram of the PSFB-SRC.

A circuit diagram of the PSFB-SRC is shown in Fig. 1. The main switches are driven by phase shift of PWM signals and it transfers input power to resonant tank. The resonant inductor L_r and the resonant capacitor C_r form the resonant tank and it generates the resonant current. The rectifier diodes rectify the resonant current. The rectified current passes through the output filter and filtered current is supplied to the load. The dynamic equations of the PSFB-SRC can be described as follows:

$$L_r \frac{di_p(t)}{dt} = v_{c_r}(t) - n \cdot v_1(t)\mathrm{sgn}(i_p(t)) + v_i(t), \tag{2}$$

$$C_r \frac{dv_{c_r}(t)}{dt} = i_p(t), \tag{3}$$

$$L \frac{di_f(t)}{dt} = v_1(t) - v_0(t), \tag{4}$$

$$C_1 \frac{dv_1(t)}{dt} = n \cdot \mathrm{abs}(i_p(t)) - i_f(t), \tag{5}$$

$$C_2 \frac{dv_0(t)}{dt} = i_f(t) - \frac{v_0(t)}{R}, \tag{6}$$

where i_p is the primary current through the inductor L_r; and v_{c_r} is the voltage across the resonant capacitor C_r. The coefficient n is the turns ratio of the transformer, $n = N_p/N_s$; v is the output voltage supplying the load; L_r is actually the sum of the resonant inductor and the leakage inductor of the transformer; and

C_r is the resonance capacitance. The resonant tank is characterized by its resonant frequency denoted by $f_0 = \frac{1}{2\pi\sqrt{L_r C_r}}$. The capacitor C_1 is used to absorb the rectified current. The inductor L and the capacitor C_2 constitute a output filter. The load is represented by a purely resistive element R.

The above system can be divided into two subsystems: resonant tank system and output filter system. The equations (2) and (3) represent the equations of resonant tank system, which consists of primary switches, resonant tank, transformer, and rectifier diodes. The equation (4)−(6) represent the equations of output filter system, which consists of output capacitance and output filter. We first analyze the operation modes of the resonant tank system, and obtain the current gain of the resonant tank system. Then, we simply rewrite the dynamics of output filter system.

Model analysis of the resonant tank system

The PSFB-SRC system has six operation modes within each switching period T_s. The operation modes are well analyzed in [9] and [10]. But, they only obtained voltage gain of the resonant tank system based on modes analysis. In the following section, we simply analyze operation modes of the converter, and obtain current gain of the resonant tank system based on modes analysis.

Steady-State analysis

Mode 1 [t_0, t_1]: Switches S_1 and S_3 are turn-on and $i_p(t)$ becomes zero. During this mode, diodes D_1, D_2 are turn-off, and so $i_s(t)$ remains zero.
Mode 2 [t_1, t_2]: At t_1, switch S_3 is turned off. After a short dead time, S_4 is turned on. Assuming that $V_{\text{in}}(t)$ and $V_1(t)$ does not vary in $t_1 \leq t < t_2$, the state equations can be written as follows:

$$L_r \frac{di_p(t)}{dt} = V_{\text{in}} - (nV_1 - v_{cr}(t)), \tag{7}$$

$$C_r \frac{dv_{cr}(t)}{dt} = -i_p(t), \tag{8}$$

$$i_p(t_1) = 0, \tag{9}$$

where $v_{\text{in}}(t) = V_{\text{in}}$ and $v_1(t) = V_1$ in $t_1 \leq t < t_2$. We also assume that power loss is almost zero. Then, $i_s(t)$ becomes $i_s(t) \simeq n i_p(t)$. $i_s(t)$ can be obtained as

$$i_s(t) = n \cdot \frac{V_{\text{in}} - (nV_1 - v_{cr}(t_1))}{Z_0} \cdot \sin w_r(t - t_1), \tag{10}$$

where

$$w_r = 2\pi f_r = \frac{1}{\sqrt{L_r C_r}}, \;\; Z_0 = \sqrt{\frac{L_r}{C_r}}. \tag{11}$$

Mode 3 [t_2, t_3]: At t_2, switch S_1 is turned off. After a dead time, S_2 is turned on at zero voltage. The state equations are the same as (7)−(9), except for the initial condition of i_s and the applied input voltage. Thus, $i_s(t)$ can be obtained analogously with (10) as

$$i_s(t) = n \cdot i_p(t_2) \cos w_r(t - t_2) - n \cdot \frac{(nV_1 - v_{cr}(t_2))}{Z_0} \cdot \sin w_r(t - t_2). \tag{12}$$

Explanations of Modes 4-6 are omitted because these modes are similar to Modes 1-3, respectively.

Current gain characteristic of the resonant tank system

The secondary current remains zero during mode 1, and the secondary current becomes zero in a short time at mode 3. Simplified waveforms are shown in Fig. 2. Neglecting modes 1 and 3 for simplicity of analysis, then we have

$$\begin{aligned} I_r(t) &= \frac{2}{T_s} \int_0^{T_s/2} i_s(\tau) d\tau, \\ &= \frac{2}{T_s} \int_0^{t_1} i_s(\tau) d\tau + \frac{2}{T_s} \int_{t_1}^{t_2} i_s(\tau) d\tau + \frac{2}{T_s} \int_{t_2}^{T_s/2} i_s(\tau) d\tau, \\ &\simeq \frac{2}{T_s} \int_{t_1}^{t_2} i_s(\tau) d\tau, \end{aligned} \tag{13}$$

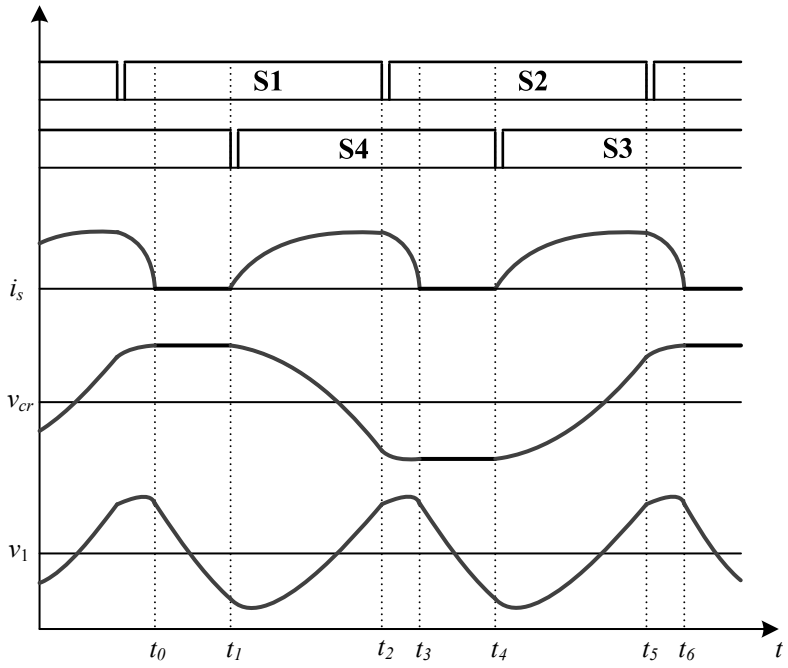

Figure 2: Simplified waveforms of i_s, v_{cr} and v_1

where $kT_s \leq t \leq (k+1)T_s$ with switching time index k. Here, we simply set $k = 0$. Substituting (10) into (13), we have

$$\begin{aligned} I_r(t) &\simeq \frac{2}{T_s}\int_{t_1}^{t_2} i_s(\tau)d\tau \\ &= \frac{2n}{T_s}\cdot\frac{V_{\text{in}}(t)-(nV_1(t)-v_{cr}(t_1))}{Z_0}\cdot\int_{t_1}^{t_1+\frac{\varphi T_s}{2}} \sin w_r(\tau-t_1)d\tau \\ &= \frac{2n}{T_s}\cdot\frac{V_{\text{in}}(t)-(nV_1(t)-v_{cr}(t_1))}{Z_0}\cdot\frac{1}{w_r}\cdot(1-\cos(\pi F\varphi)), \end{aligned} \tag{14}$$

where, $F = f_r/f_s$. As $v_{cr}(t_1)$ can be substituted as $\frac{I_r(t)}{2nC_rf_s}$ in the mode 2, so

$$\begin{aligned} I_r(t) &= 2nC_rf_s(V_{\text{in}}(t)-nV_1(t)+\frac{I_r(t)}{2nC_rf_s})\cdot(1-\cos(\pi F\varphi)) \\ &= (2nC_rf_sV_{\text{in}}(t)-2n^2C_rf_sV_1(t)+I_r(t))\cdot(1-\cos(\pi F\varphi)), \end{aligned} \tag{15}$$

where φ is phase shift value. It follows from (15) that

$$I_r(t) = g_1(\varphi) = \frac{(2nC_rf_sV_{\text{in}}(t)-2n^2C_rf_sV_1(t))\cdot(1-\cos(\pi F\varphi))}{\cos(\pi F\varphi)}. \tag{16}$$

Equation (16) is the phase-shift value/current relationship. Except for cosine terms, the terms on the right side hand of (16) are almost constant because the values of the resonance capacitance hardly vary. But, due to the cosine terms existing in the denominator and numerator, this relationship becomes highly nonlinear.

In what follows, we derive current/phase-shift value relationship which can be used to construct nonlinear

compensator. Rearranging (16) for φ, we have

$$\begin{aligned}\cos(\pi F\varphi) &= 1-\frac{I_r(t)}{2nC_rf_sV_{\text{in}}(t)-2n^2C_rf_sV_1(t)+I_r(t)}\\ &= \frac{2C_rf_sV_{\text{in}}(t)-2nC_rf_sV_1(t)}{2C_rf_sV_{\text{in}}(t)-2nC_rf_sV_1(t)+\frac{I_r(t)}{n}}.\end{aligned} \tag{17}$$

Multiplying inverse of cosine function and dividing πF on the both sides of (17), we have

$$\varphi = g_1^{-1}(I_r(t)) = \frac{1}{\pi F}\cos^{-1}\left(\frac{2C_rf_sV_{\text{in}}(t)-2nC_rf_sV_1(t)}{2C_rf_sV_{\text{in}}(t)-2nC_rf_sV_1(t)+\frac{I_r(t)}{n}}\right). \tag{18}$$

Model analysis of the output filter system

In the output filter system, the rectified current i_r and the output voltage v_o are taken as the input signal and output signal for the output filter system, respectively; and then, (4)-(6) can be rewritten as:

$$L\frac{di_f(t)}{dt} = -v_1(t)-v_0(t), \tag{19}$$

$$C_1\frac{dv_1(t)}{dt} = I_r(t)-i_f(t), \tag{20}$$

$$C_2\frac{dv_0(t)}{dt} = i_f(t)-\frac{v_0(t)}{R}. \tag{21}$$

Remark 1. The resonant tank and the output filter systems are quite different in their electric inertia. The time constant for resonant tank system needs to be set to satisfy $f_r \simeq f_s$ and $f_r \leq f_s$. The time constant of the output filter needs to be much greater than that of the resonant tank to smooth the resonant current. As a result, the resonant tank system and output filter system can be considered as a static nonlinearity and system dynamics each.

Controller design

Problem formulation

Defining $x_1(t) = v_o(t)$, $x_2(t) = \frac{1}{C_2}i_f(t) - \frac{1}{RC_2}v_o(t)$, $x_3(t) = -\frac{1}{LC_2}v_1(t) - \frac{1}{RC_2^2}i_f(t) + \left(\frac{1}{R^2C_2^2} - \frac{1}{LC_2}\right)v_o(t)$, the dynamic equations (19)-(21) can be rewritten as the nonlinear systems in the normal form

$$\begin{aligned}\dot{x}_1(t) &= x_2(t),\\ \dot{x}_2(t) &= x_3(t),\\ \dot{x}_3(t) &= f(\mathbf{x}(t)) + g_2\cdot g_1(u(t)) + d(t),\\ &= f(\mathbf{x}(t)) + g(u(t)) + d(t),\\ y(t) &= x_1(t),\end{aligned} \tag{22}$$

where $\mathbf{x} = [x_1(t), x_2(t), x_3(t)]^T \in R^{3\times 1}$ is a state vector, $u(t) \in R^1$ is a control input, $f(\mathbf{x}(t))$ and $g(\cdot) = g_2\cdot g_1(\cdot)$ are the system function and the control gain respectively, representing nonlinear functional relationships, and $d(t)$ is a unknown unexpected nonlinear term; $f(\mathbf{x}(t))$ and g_2 are represented as

$$\begin{aligned}f(\mathbf{x}(t)) &= f_n(\mathbf{x}(t)) + \Delta f(\mathbf{x}(t)),\\ g_2 &= g_{2n} + \Delta g_2,\end{aligned} \tag{23}$$

where the nominal system function $f_n(\mathbf{x}(t))$ and the nominal control gain g_{2n} are represented as

$$f_n(\mathbf{x}(t)) = -\frac{1}{RC_2}x_3(t) - \frac{1}{L}(\frac{1}{C_1}+\frac{1}{C_2})x_2(t) - \frac{1}{RC_1C_2L}x_1(t), \tag{24}$$

$$g_{2n} = \frac{1}{C_1C_2L}, \tag{25}$$

and the system uncertainty $\Delta f(\mathbf{x}(t))$ and control gain uncertainty Δg_2 satisfies the following inequalities

$$|\Delta f(\mathbf{x}(t))| < F,$$
$$0 < g_{2,min} \leq g_2 = g_{2n} + \Delta g_2 \leq g_{2,max},$$

where $g_{2,min}$ and $g_{2,max}$ are given positive constants. Since the control input $u(t)$ is multiplied by the inverse of control gain in the following section, the control gain g_2 needs to be estimated as the geometric mean of the lower and upper bounds of control gain g_2:

$$\hat{g}_2 = \frac{1}{\sqrt{g_{2,min} \cdot g_{2,max}}}. \tag{26}$$

Also, $d(t)$ is bounded as

$$|d(t)| < D,$$

where D is the upper bound of nonlinear loads. Nonlinearity $g_1(\cdot)$ and variation of parameter R, nonlinear loads R_L and C_L may degrade the control performance and even cause the system to become unstable. To overcome this problem, we propose 3-SMC in the following section.

Controller design

The main idea of 3-SMC is to constrain an PSFB-SRC system to reach and stay on both a sliding surface $s(t)$ and first time-derivative of the surface $\dot{s}(t)$; $s(t) = \dot{s}(t) = 0$ after a finite time, and thereby the error variables moves on the prescribed error dynamics. We start with choosing the 3-SMC, which is well known for its robustness to parameter uncertainties and nonlinearity. The third-order sliding surface is given as

$$s(t) = (\frac{d}{dt} + \lambda)^2 e(t) = \lambda^2 e(t) + 2\lambda \dot{e}(t) + \ddot{e}(t), \tag{27}$$

where $e(t) = x_{1d}(t) - x_1(t) \in \mathrm{R}$ represents the tracking error, $\lambda \in \mathrm{R}$ is a positive constant. Substituting (22) into (27) yields

$$\dot{s}(t) = \lambda^2 \dot{e}(t) + 2\lambda \ddot{e}(t) + \dddot{x}_{1d}(t) - (f(\mathbf{x}(t)) + g(u(t)) + d(t)). \tag{28}$$

Let the equivalent control law be

$$u_{eq}(t) = g_1^{-1}(\hat{g}_2^{-1}(\lambda^2 \dot{e}(t) + 2\lambda \ddot{e}(t) + \dddot{x}_{1d}(t) - f_n(\mathbf{x}(t)))), \tag{29}$$

where λ are chosen such that the polynomial $\dddot{e}(t) + 2\lambda \ddot{e}(t) + \lambda^2 \dot{e}(t)$ becomes a Hurwitz polynomial. Applying the control law (29) into (28) yields

$$\begin{aligned}
\dot{s}(t) &= \lambda^2 \dot{e}(t) + 2\lambda \ddot{e}(t) + \dddot{e}(t) \\
&= \lambda^2 \dot{e}(t) + 2\lambda \ddot{e}(t) + \dddot{x}_{1d}(t) - (f(\mathbf{x}(t)) + g(u(t)) + d(t)), \\
&= \lambda^2 \dot{e}(t) + 2\lambda \ddot{e}(t) + \dddot{x}_{1d}(t) - f(\mathbf{x}(t)) \\
&\quad - g(g_1^{-1}(\hat{g}_2^{-1}(\lambda^2 \dot{e}(t) + 2\lambda \ddot{e}(t) + \dddot{x}_{1d}(t) - f_n(\mathbf{x}(t))))) - d(t) \\
&= (\lambda^2 \dot{e}(t) + 2\lambda \ddot{e}(t) + \dddot{x}_{1d}(t) - f(\mathbf{x}(t)))(1 - g_2 \cdot \hat{g}_2^{-1}) - (f(\mathbf{x}(t)) - f_n(\mathbf{x}(t)))g_2 \cdot \hat{g}_2^{-1} - d(t) \\
&\leq |\lambda^2 \dot{e}(t) + 2\lambda \ddot{e}(t) + \dddot{x}_{1d}(t) - f(\mathbf{x}(t))| \cdot |1 - g_2 \cdot \hat{g}_2^{-1}| + |f(\mathbf{x}(t)) - f_n(\mathbf{x}(t))| \cdot |g_2 \cdot \hat{g}_2^{-1}| + |d(t)|.
\end{aligned} \tag{30}$$

Therefore, the resulting error dynamics satisfies the inequality

$$\begin{aligned}
\dot{s}(t) &= \lambda^2 \dot{e}(t) + 2\lambda \ddot{e}(t) + \dddot{e}(t) \\
&\leq U|1 - \beta| + F \cdot \beta + D,
\end{aligned} \tag{31}$$

where

$$|\lambda^2\dot{e}(t)+2\lambda\ddot{e}(t)+\dddot{x}_{1d}(t)-(f(\mathbf{x}(t))|<U \tag{32}$$

$$|g_2\cdot\hat{g}_2^{-1}|<\beta;\ |f(\mathbf{x}(t)-f_n(\mathbf{x}(t))|<F;\ |d(t)|<D. \tag{33}$$

If the bias term $U|1-\beta|+F\cdot\beta+D$ becomes zero, then we obtain the ideal error dynamics

$$\dot{s}(t)=\lambda^2\dot{e}(t)+2\lambda\ddot{e}(t)+\dddot{e}(t)=0. \tag{34}$$

However, the bias term $U|1-\beta|+F\cdot\beta+D$ prevents the tracking error e from being zero. To suppress this bias term, we adopt the switching control input as:

$$u_{sw}(t)=g_1^{-1}(\hat{g}_2^{-1}k_{sw}\mathrm{sgn}(s(t))), \tag{35}$$

where $k_{sw}\in\mathrm{R}$ is positive constants and satisfies inequality $k_{sw}\geq\frac{U|1-\beta|+F\cdot\beta+D+\eta}{g_{2,min}\cdot\hat{g}^{-1}}$ where $\eta\in\mathrm{R}$ is a positive constant. Combining the equivalent and switching control laws, we have the complete control law as:

$$\begin{aligned}u(t)&=u_{eq}(t)+u_{sw}(t)\\&=g_1^{-1}(\hat{g}_2^{-1}(\lambda^2\dot{e}(t)+2\lambda\ddot{e}(t)+\dddot{x}_{1d}(t)-f_n(x(t))))+g_1^{-1}(\hat{g}_2^{-1}k_{sw}\mathrm{sgn}(s(t))).\end{aligned} \tag{36}$$

Remark 2. Assuming that the coefficients of the state equations (24) and (25) may fluctuate up to 50% from their nominal values, the bounds of the uncertainties and the estimation error can be determined: The sliding mode switching control law guarantees that the sliding condition is satisfied even in the presence of model uncertainties and unknown disturbances. Discontinuous switching control usually results in chattering, which may excite undesirable high frequencies or unmodeled dynamics. Chattering can be alleviated by a smoothing approximation in the boundary layer neighboring the sliding surface, $s(t)=0$. A simple method is to replace a sign function with the following saturation function (Utkin et al., 1999):

$$\mathrm{sgn}(s(t))\rightarrow\mathrm{sat}(s(t)/\phi) \tag{37}$$

where $\phi>0$ represents the thickness of the boundary layer, which should be adjusted to achieve an optimal balance of tracking performance and chatter reduction. The resulting control law is written as follows:

$$\begin{aligned}u(t)=\varphi=&g_1^{-1}(\hat{g}_2^{-1}(\lambda^2\hat{e}(t)+2\lambda\ddot{e}(t)+\dddot{x}_{1d}(t)-f_n(x(t))))\\&+g_1^{-1}(\hat{g}_2^{-1}\cdot k_{sw}\mathrm{sat}(s(t)/\phi)).\end{aligned} \tag{38}$$

In this control law, chattering is alleviated even though $s(t)$ may not tend towards zero. The resulting control law guarantees that the solution of the closed-loop system will reach the boundary layer within a finite time t_r and remain ultimately bounded in the neighborhood of the origin.

Simulation

To demonstrate the feasibility of the developed controller, a simulation is conducted to evaluate the performance of the 3-SMC fo PSFB-SRC.
The dynamics of PSFB-SRC are given as

$$\begin{aligned}\dot{x}_1(t)&=x_2(t),\\\dot{x}_2(t)&=x_3(t),\\\dot{x}_3(t)&=-\frac{1}{RC_2}x_3(t)-\frac{1}{L}(\frac{1}{C_1}+\frac{1}{C_2})x_2(t)-\frac{1}{RC_1C_2L}x_1(t)\\&\quad+\frac{1}{C_1C_2L}\cdot\frac{(2nC_rf_sV_{\mathrm{in}}-2n^2C_rf_sV_1+I_r(t))\cdot(1-\cos(\pi F\varphi))}{\cos(\pi F\varphi)}\\&\quad+\Delta f(x(t))+\Delta g_2\cdot g_1(u(t))+d(t),\end{aligned} \tag{39}$$

where we set the input voltage V_{in}=300 V, the desired output voltage V_d=100 V, the resonance inductance L_r=100 μH, the resonance capacitance C_r=0.47 μF, the capacitance C_1=0.47 μF, the capacitance C_2=100

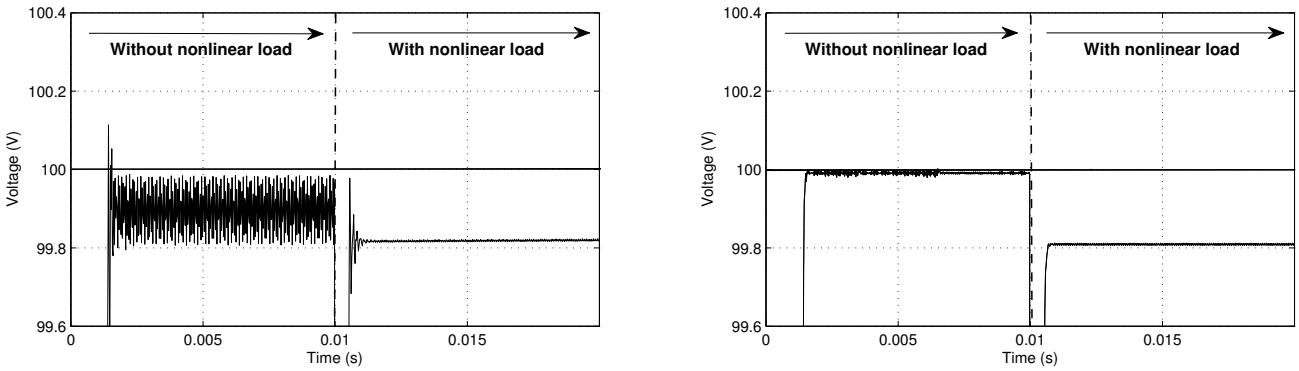

(a) (b)

Figure 3: The waveforms of output voltage (left) and duty ratio (right) when the conventional proportional-integral (PI) controller is used.

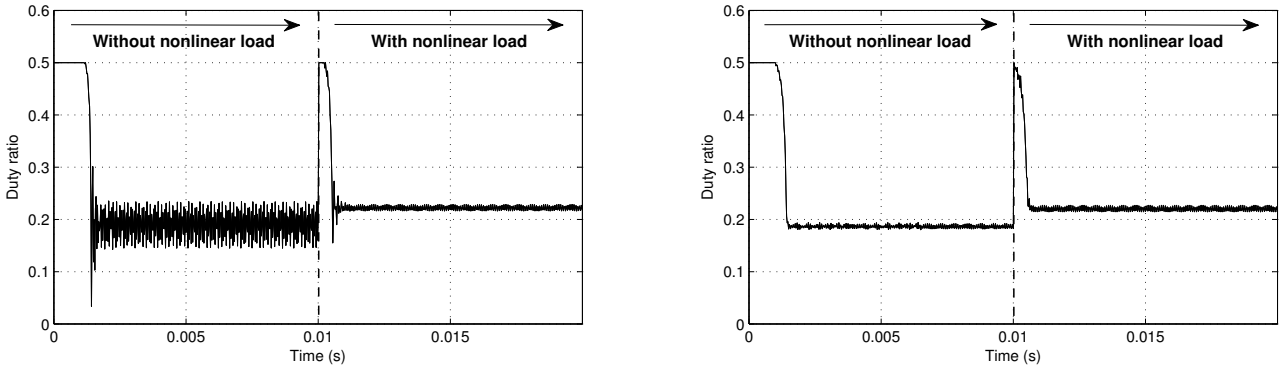

(a) (b)

Figure 4: The waveforms of output voltage (left) and duty ratio (right) when the proposed 3-SMC is used.

μF, the inductance L=200 μH, switching frequency f_s=33 kHz, nonlinear load resistance and capacitance R_L=200 Ω, C_L=20 uF, respectively. We set also λ=500, the switching control gain k_{sw}=1350, and the estimated control gain $\hat{g}_2$=$1.064 \cdot 10^{14}$. We simulate this example for 0.03 s with power electric simulation software (PSIM).

Under the above settings and unit step input command ($V_d = 100\ V$), we applied linear controller and 3-SMC to PSFB-SRC. For the first 0.01s and last 0.01 s with resistive load 100 Ω, the transient and steady-state response with 3-SMC is much better than that with linear controller (Figs. 3, 4). From $t = 0.01$ to $t = 0.02$ s, the nonlinear load R_L=200 Ω, C_L=20 uF is used. In this case, 3-SMC also performs better than the linear controller. The control input profiles are shown in Figs. 3, 4.

Table I: RMS errors

Controller	Without nonlinear load	With nonlinear load
Conventional PI controller	0.1071	2.1890
Proposed 3-SMC	0.0126	2.1594

Conclusion

In this paper, a third-order sliding mode control (3-SMC) scheme is proposed for the PSFB-SRC which has a nonlinear characteristic. Conventional controller cannot compensate for the nonlinear load variation due to the nonlinear characteristic of PSFB-SRC. However, 3-SMC can effectively suppress this variation with compensating the nonlinear characteristic of PSFB-SRC. Nonlinear characteristic of resonant tank

system and the dynamics of output filter are derived. Simulation results verify the feasibility of proposed controller.

Acknowledge

This research was supported by the MSIP(Ministry of Science, ICT and Future Planning), Korea, under the "ICT Consilience Creative Program" (IITP-2015-R0346-15-1007) supervised by the IITP(Institute for Information & communications Technology Promotion).

References

[1] Sable, D. M., & Lee, F. C.: The operation of a full-bridge zero-voltage-switched PWM converter, VPEC Seminar 89, 92-97, 1989.
[2] Forsyth, A. J., Evans, P. D., Cheng, K. W. E., & Al-Mothafar, M. R. D.: Operating limits of power converters for high power ion engine control, 22nd International Electric Propulsion Conference, 1991.
[3] Sullivan, C. R., Awerbuch, J. J., & Latham, A. M.: Decrease in photovoltaic power output from ripple: Simple general calculation and the effect of partial shading, Power Electronics, IEEE Transactions on, 28(2), 740-747, 2013.
[4] Gemmen, R. S.: Analysis for the effect of inverter ripple current on fuel cell operating condition, Journal of fluids engineering, 125(3), 576-585, 2003.
[5] Zhang, B., Wang, D., Zhou, K., & Wang, Y.: Linear phase lead compensation repetitive control of a CVCF PWM inverter, Industrial Electronics, IEEE Transactions on, 55(4), 1595-1602., 2008.
[6] Tzou, Y. Y., Jung, S. L., & Yeh, H. C.: Adaptive repetitive control of PWM inverters for very low THD AC-voltage regulation with unknown loads, ower Electronics, IEEE Transactions on, 14(5), 973-981, 1999.
[7] Garcia-Cerrada, A., Pinzon-Ardila, O., Feliu-Batlle, V., Roncero-Sanchez, P., & Garca-Gonzlez, P.: Application of a repetitive controller for a three-phase active power filter, Power Electronics, IEEE Transactions on, 22(1), 237-246, 2007.
[8] Chan, H. L., Cheng, K. W. E., & Sutanto, D.: ZCSZVS bi-directional phase-shifted DCDC converter with extended load range, IEE Proceedings-Electric Power Applications, 150(3), 269-277, 2003.
[9] Lee, W. J., Kim, C. E., Moon, G. W., and Han, S. K.: A new phase-shifted full-bridge converter with voltage-doubler-type rectifier for high-efficiency PDP sustaining power module, Industrial Electronics, IEEE Transactions on, 55(6), 2450-2458, 2008.
[10] Kim, E. H., and Kwon, B. H.: Zero-voltage-and zero-current-switching full-bridge converter with secondary resonance, Industrial Electronics, IEEE Transactions on, 57(3), 1017-1025, 2010.
[11] Xu, D., Zhao, C., & Fan, H.: A PWM plus phase-shift control bidirectional DC-DC converter, Power Electronics, IEEE Transactions on, 19(3), 666-675, 2004.
[12] Feng, C., Liang, J., & Agelidis, V. G.: Modified phase-shifted PWM control for flying capacitor multilevel converters, Power Electronics, IEEE Transactions on, 22(1), 178-185, 2007.
[13] SiraRamrez, H., Ortega, R., & GarcaEsteban, M.: Adaptive passivitybased control of average dctodc power converter models, International journal of adaptive control and signal processing, 12(1), 63-80, 1998.
[14] Jacobson, C. A., Stankovic, A. M., & Tadmor, G. Design of robust controllers for resonant DC/DC converters. In Proc. IEEE Conf. Control Applications, 360-365, September 1995.
[15] Lu, Y., Cheng, K. W. E., & Ho, S. L.: Auto-disturbance-rejection control for phase-shifted resonant converter, In Electric Power Applications, IEE Proceedings (Vol. 153, No. 5, pp. 711-718). IET, September 2006.
[16] Lu, Y., Cheng, K. W. E., Ho, S. L., & Pan, J. F.: Passivity-based control of a phase-shifted resonant converter, IEE Proceedings-Electric Power Applications, 152(6), 1509-1515, 2005.
[17] Slotine, J. J. E.: Sliding controller design for non-linear systems, International Journal of control, 40(2), 421-434, 1984.
[18] Park, K. B., & Lee, J. J.: Sliding mode controller with filtered signal for robot manipulators using virtual plant and controller, Mechatronics, 7(3), 277-286, 1997.
[19] Fridman, L., & Levant, A.: Higher order sliding modes, Sliding mode control in engineering, 11, 53-102, 2002.
[20] Levant, A.: Higher-order sliding modes, differentiation and output-feedback control, International journal of Control, 76(9-10), 924-941, 2003.
[21] Laghrouche, S., Plestan, F., & Glumineau, A.: Higher order sliding mode control based on integral sliding mode, Automatica, 43(3), 531-537, 2007.